Thermal Conductivity of Liquid/CNT Core-Shell Nanocomposites

Yutaka Yamada,[1,a)] Alexandros Askounis,[2] Tatsuya Ikuta,[2,3] Koji Takahashi,[2,3,4] Yasuyuki Takata,[2,4,5] and Khellil Sefiane,[6,7]

[1]*Graduate School of Natural Science and Technology, Okayama University, Okayama 700-8530, Japan*

[2]*International Institute for Carbon-Neutral Energy Research (WPI-I2CNER), Kyushu University, Fukuoka 819-0395, Japan*

[3]*Department of Aeronautics and Astronautics, Graduate School of Engineering, Kyushu University, Fukuoka 819-0395, Japan*

[4]*Japan Science and Technology Agency (JST), CREST, Kyushu University, Fukuoka 819-0395, Japan*

[5]*Department of Mechanical Engineering, Graduate School of Engineering, Kyushu University, Fukuoka 819-0395, Japan*

[6]*Institute for Materials and Processes, School of Engineering, The University of Edinburgh, King's Buildings, Robert Stevenson Road, Edinburgh EH9 3FB, UK*

[7]*Tianjin Key Lab of Refrigeration Technology, Tianjin University of Commerce, Tianjin City, 300134, PR China*

ABSTRACT

Hollow carbon nanotubes (CNTs) were impregnated with an ionic liquid, resulting in a composite core-shell nanostructure. Liquid infusion was verified by transmission electron microscopy and rigorous observations unveiled that the nanocomposite is stable, *i.e.* liquid did not evaporate owing to its low vapor pressure. A series of individual nanostructures were attached on T-type heat sensors and their thermal behavior was evaluated. The liquid core was found to reduce the thermal conductivity of the base structure, CNT, from *ca.* 28 W/mK to *ca.* 15 W/mK. These findings could contribute to a better understanding of nanoscale thermal science and potentially to applications such as nanodevices thermal management and thermoelectric devices.

I. INTRODUCTION

Carbon nanotubes (CNTs) are typical one-dimensional building materials resembling individual or multiple graphene sheets rolled up into cylinders[1,2]. Due to their size and structure, CNTs exhibit unique properties such as high mechanical strength[3], chemical inertness[4] and high electrical conductivity[5,6]. The thermal properties of individual CNTs, in particular, have attracted considerable scientific attention as they exhibit extremely high thermal conductivity[7-9], with the effect of CNT length[10], diameter[11,12], defects

[a)] Author to whom correspondence should be addressed. Electronic mail: y.yamada@okayama.ac.jp

and wall structure[13,14] also carefully considered. Potentially, CNTs could be employed in high heat flux applications like nanodevices thermal management[15] and/or low heat transport applications like thermoelectric devices[16].

Heat conduction occurs mainly via the CNTs wall rendering the inner, hollow space useless. This space may be utilized for enhancing or reducing heat conduction by the insertion of a second material which leads to a core-shell nanocomposite. This is a promising approach as allows the tailoring of the nanocomposite properties to the application needs without the introduction of defects which may result in degradation of the nanocomposite. Although, CNTs infusion with a liquid core has been reported experimentally[17,18]; little is known about the effect of this infusion on the nanocomposite thermal behavior, with even theoretical works rather limited[19]. Previous experimental studies have mainly focused on a heterostructures which have solid core and solid shell, and the thermal and thermoelectric performance of core-shell Te−Bi[20,21] and Si-Ge[22,23] nanowires.

In this paper, we develop a novel core-shell nanocomposite consisting of a liquid core fused inside a CNT shell structure, confirmed by transmission electron microscopy (TEM). The nanocomposite is then attached on a nanofilm heat sensor and its thermal conductivity is measured and compared to that of the base material (CNT). This is the first, to the best of our knowledge, experimental measurement of the thermal conductivity of liquid filled CNTs.

II. EXPERIMENTAL

The heat nanosensors consisted of a platinum nanofilm suspended on a silicon oxide surface were fabricated using typical microelectromechanical systems (MEMS) processes. The exact fabrication procedure is described in detail elsewhere[9,24]. A scanning electron microscope (SEM; Versa 3D, FEI Co., Hillsboro, OR, USA) allowed the characterisation of the sensors, with typical 9 μm length, 500 nm width

and 40 nm thickness. In the present study, open-ended, hollow, multi-walled CNTs (US Nanomaterials; Houston, TX, USA) were selected due to the difficulty of manipulating single-walled CNTs. A small amount of these CNTs was dispersed in ethanol and gently dropped on a transmission electron microscopy (TEM) copper microgrid (Ouken Shoji Inc., Japan). Grids were left to dry for 12 hours. Individual CNTs were characterized by high-resolution TEM (JEM-3200FSK; JEOL Ltd., Japan) operating at an accelerating voltage of 300 kV. A series of CNTs have been measured and Figure 1(a) shows the micrograph of a typical CNT measured in this study, with *ca.* 83 and 45 nm outer and inner diameter, respectively, and *ca.* 6 μm length. Subsequently, the CNTs were impregnated with the ionic liquid (IL) 1-Butyl-3-methylimidazolium hexafluorophosphate (Kanto Chemical Co., Tokyo, Japan) by depositing a droplet of the liquid on the microgrid with the CNTs and it spun at 6000 rpm for 1 minute to remove residual liquid after waited 10 seconds to introduce the liquid into CNTs. This ionic liquid (IL) was chosen due to: a) its extremely low vapor pressure; no evaporation under electron microscopy vacuum[25] and b) the surface tension of this IL was reported to be *ca.* 44 mN/m[26], which is well below the surface tension cut-off value reported to be in the range of 100 - 200 mN/m for CNT wetting and filling[17,18,27]. TEM observation of a series of CNTs verified the successful impregnation of CNTs with IL; a micrograph of a characteristic IL filled CNT is presented in Figure 1(b), with *ca.* 85 and 46 nm as an outer and inner diameter, respectively. Notably, a number of gas bubbles were observed within the CNT, as pointed in Figure 1(b), potentially due to slug flow during the capillary filling, in accordance with the literature[28,29] or dissolved gases which emerged in high vacuum condition. The bubbles are not in contact with the CNT walls due to the high viscosity of IL. Bubble volume fraction was estimated to be *ca.* 5 % and is therefore not considered.

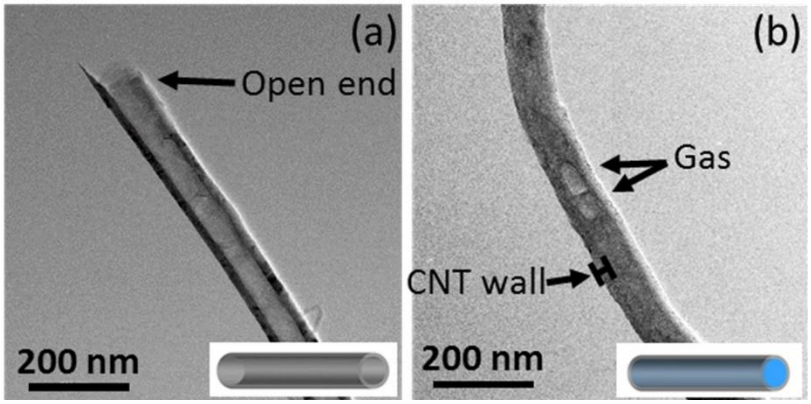

Figure 1 (a) TEM micrograph depicting part of an empty CNT. (b) TEM micrograph depicting a typical IL-CNT core-shell nanostructure.

With the help of a manipulation in SEM, individual nanostructures were weakly bonded on the nanotip of a metallic needle via focused electron beam induced deposition. Subsequently, the nanostructures were attached first on the nanosensor (NS) and then to the heat sink (HS), as shown in Figure 2 for an IL/CNT nanocomposite. A constant current was supplied to the NS which acts simultaneously as a heater and a thermometer. Thus, we are capable of maintaining the whole system at a constant temperature T_0.

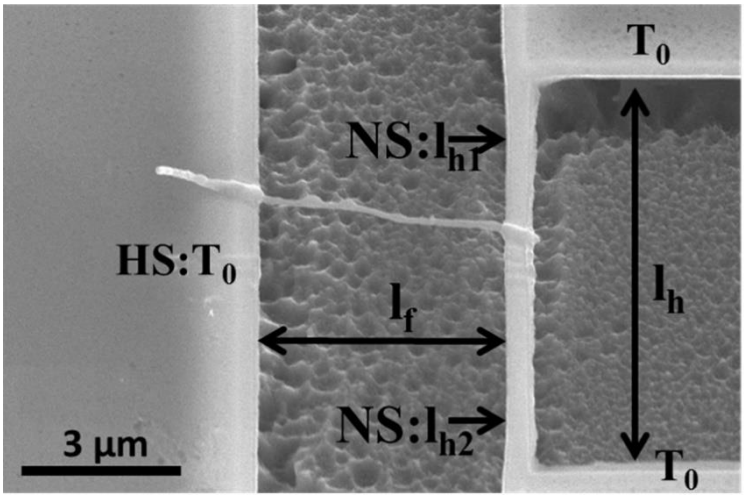

Figure 2 SEM micrograph depicting the T-type heat nanosensor with an attached IL/CNT core-shell nanostructure.

III. RESULTS AND DISCUSSION

Our system allows the direct measurement of the volumetric heat generation rate, q_v, which is given by $q_v = IV/(wtl_h)$, where I, V, w and t are the heating current, voltage at the NS, width and thickness of the nanofilm (NS in Figure 2), respectively. Since our measurements are conducted under the high vacuum conditions of an SEM and the temperature rise was small, both radiation and convection thermal transport are negligible.[9] The thermal conductivity of each nanostructure is thus calculated using the following formula:[9]

$$\lambda_f = \frac{l_f l_h \lambda_h A_h (l_h^3 q_v - 12 l_h \lambda_h \Delta T_v)}{l_{h1} l_{h2} A_f \left\{12 l_h \lambda_h \Delta T_v - q_v (l_{h1}^3 + l_{h2}^3)\right\}} \quad (1)$$

where each quantity is represented in Figure 2. A_h and A_f are the nanofilm and CNT cross-sectional area, l_f is the length of the CNT between NS and HS, l_h is the total length of the NS, l_{h1} and l_{h2} are the lengths between the CNT junction and the edge of the NS and λ_h is the nanofilm (NS) thermal conductivity. ΔT_v is obtained from $\Delta T_v = \Delta R/(\beta R_0)$, where R_0 is the nanofilm electrical resistance measured at 0°C, ΔR is the electrical resistance change during heating and β the resistance-temperature coefficient of the nanofilm as measured during the calibration of the sensor. Figure 3 shows the thermal conductivity as a function of temperature for the shell (open symbols) and the core-shell (closed symbols) nanostructures, respectively. In this case the thermal contact resistance, which has been reported to be small compare to the CNT thermal resistance, was kept to a minimum by minimizing the shell-sensor junction and depositing an extra layer of amorphous carbon via SEM[7,9,30]. Hence, the thermal conductivities reported here correspond to the lower bound of the actual intrinsic thermal conductivities of the nanostructures. The shell nanostructure (CNT) exhibits a $\lambda_f \approx 28$ W/mK (open symbols) which is considerably lower than previous reports for similar sized CNTs[11,13] but still in line with the literature for this type of CNTs[31,32].

In fact, the walls of these CNTs consist of graphene layers rolled up into cones and stacked one inside the other giving rise to the cup-stacked wall structure[33], as shown in Figure 4. Each graphene layer is inclined a few degrees relative to the longitudinal tube axis. The effect of this wall structure on the thermal transport of the CNT is discussed elsewhere[32]. Defects and interlayer covalent bonding are expected to lower the thermal conductivity, however high-resolution TEM showed a minimal amount.

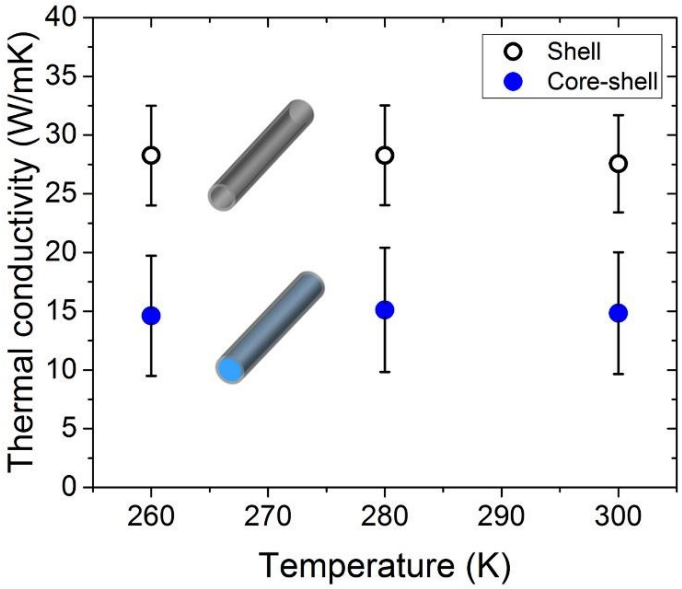

Figure 3 Thermal conductivity, λ_f , as function of temperature for the shell (open symbols) and the core-shell (closed symbols) nanostructure.

It is readily apparent from Figure 3 (closed symbols) that the liquid core lowers the thermal conductivity of the nanocomposite from *ca.* 28 W/mK to *ca.* 15 W/mK. We shall attempt to address this decrease by combining conventional 1-D heat conduction in composite materials and phonon heat conduction mechanism arguments. Heat is conducted following one-dimensional Fourier's law $q = -kA\,dT/dz$, with the heat flow q in the axial z direction and dT/dz the temperature gradient[34]. This approach is fundamental to the accurate determination of thermal transport in nanostructures and shows the need for a precise definition of the CNT cross-sectional area, which remains ambiguous in most experimental

studies due to limitations in measuring the inner wall diameter[35]. The heat conduction path should, thus, encounter a thermal resistance in the composite equivalent to[34]:

$$\frac{1}{R_{comp}} = \frac{1}{R_{core}} + \frac{1}{R_{shell}} \tag{2}$$

where R_{comp}, R_{core} and R_{shell} correspond to the thermal resistance of the composite, the liquid core (IL) and the shell (CNT), respectively. Generally, the thermal conductivity and thermal resistance are related by: $R = L/\lambda A$, with heat conduction length L, thermal conductivity λ and surface of conduction A, which substituted in Eq. (2) yields the effective thermal conductivity of our liquid-core composite:

$$\lambda_{eff} = \frac{\lambda_{core} A_{core} + \lambda_{shell} A_{shell}}{A_{tot}} \tag{3}$$

where, the thermal conductivity of the core λ_{core} is assumed to be 0.2 W/mK[36,37]. We used this bulk value due to a lack of more detailed data in the literature for this particular IL, which should act as the foundation for our comparison. Additionally, no particular confinement effect is expected, since the tubular area in our CNT is considerably larger than that of a thin CNT, where the available space in the tube and the hydrogen bond length become comparable[38,39]. The thermal conductivity of the shell λ_{shell} was measured to be 28 W/mK and A_{tot} is the total conducting surface of the composite expressed as: $A_{tot} = A_{shell} + A_{core} = \pi r_o^2$, where A_{shell} and A_{core} are the cross sectional area of CNT wall and core liquid, respectively. Eq. 3 yields an effective thermal conductivity for the composite $\lambda_{eff} \approx 19.9$ W/mK. The lower λ_{eff} value can be obtained when λ_{core} is lower than λ_{shell}, and this result shows that the thermal resistance of the sample increased after liquid insertion. Hence, we may conclude that the liquid core is acting as a thermal resistance. To further support this claim, we calculate λ_{shell}, using the measured λ_{eff} of the composite, to be approx. 21 W/mK from Eq. (3). This result is smaller than the measured λ_{shell}, which is further evidence of the infused liquid acting as a thermal resistance. Moreover, these calculations show the importance of accurately defining the cross-sectional area for heat conduction, which is further

supported when considering phonon heat conduction in nanostructures. Nonetheless, these values are close but not equal to the measured one.

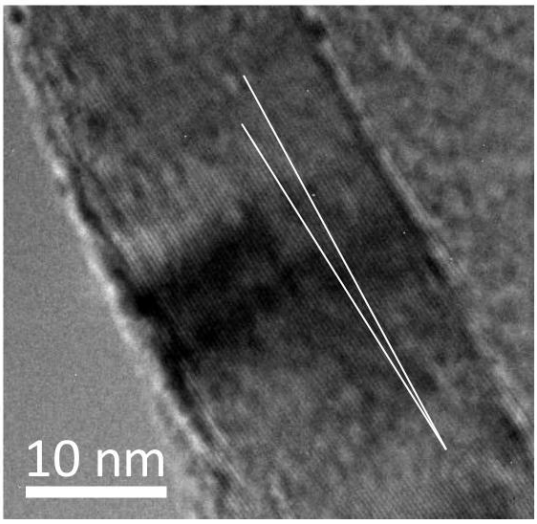

Figure 4 Typical TEM micrograph depicting the inclined wall structure of the CNTs in this work.

This discrepancy shows the limitation of the conventional heat conduction mechanism for nanomaterials[10, 40-42], leading us to further consider the limiting factors of phonon-phonon and phonon boundary scattering, as phonons are the main energy carrier regardless of diameter (for a comprehensive review see Ref. 35). In fact, Chang et al., reported a similar deviation of the thermal conductivity of carbon and boron nanotubes from Fourier's law due to isotopic deviations[10]. Nonetheless, Fourier's law remains a useful tool to approximate the effective thermal conductivity of nanomaterials. For example, Thomas et al. predicted, based on Fourier's law[19], a decrease in the effective thermal conductivity of a single-walled carbon nanotube when a liquid core was inserted. In particular, they estimated that the vibrational frequency of the water atoms coincides with the low vibrational frequencies of the acoustic phonons. Therefore, interactions between the two should lead to phonon scattering and in turn to a decrease in the thermal conductivity of the composite[19]. Our experimental results are complementary to this theoretical work, therefore we expect a similar thermal transport mechanism to be at work, with the additional effect

of the unique wall structure. Fig. 4 depicts this unique structure and the white line highlight the inclination of the graphene layers in relation to the tube axis. This inclination has a significant effect on the heat transport of the core structure as the phonons follow the ballistic regime within each graphene layer and the diffusive across the tube length, as we have discussed in detail elsewhere[32]. The composite thermal transport should also be affected by this unique wall structure. Specifically, more graphene edges are in contact with the liquid which should amount to a higher amount of phonon scattering giving rising to the observed discrepancy. This argument merits further exploration in the future.

IV. SUMMARY AND CONCLUSIONS

To summarize, we have successfully prepared a liquid-core nanocomposite. Using a thin film heat nanosensor we evaluated the thermal conductivity of the nanocomposite and its base structure a CNT. A decrease in the thermal conductivity of the nanocomposite was found and it was lower than the result predicted by bulk scale theory, due to phonon interaction with the liquid molecules. This is the first, to the best of our knowledge, experimental evidence of a liquid/CNT core-shell nanocomposite and its thermal behavior assessment. We believe that these results contribute to a better understanding of nanoscale thermal transport. Additionally, we provided experimental evidence and quantification of heat transfer at the solid-liquid interface of nanocomposites. Potentially, our results could pave the way for further research into nanoscale phase change phenomena, chemical reactions, fluid flows and thermoelectrics in CNTs.

ACKNOWLEDGEMENTS

We acknowledge the Japan Society for the Promotion of Science (JSPS) for the Postdoctoral Fellowship for North American and European Researchers. This work was financially supported in part by the Core Research for Evolutional Science and Technology project of Japan Science and Technology Agency (JST-

CREST). We are also grateful to the research laboratory for High Voltage Electron Microscopy at Kyushu University, for use of the TEM facilities.

Author information

*Corresponding Author
Yutaka Yamada
Tel.: +81-86-251-8046; Fax: +81-86-251-8266;
E-mail: y.yamada@okayama-u.ac.jp

Notes

The authors declare no competing financial interest.

References

1 S. Iijima, Nature **354**, 56 (1991).
2 S. Iijima, and T, Ichihashi, Nature **363**, 603 (1993).
3 B. I. Yakobson, C. J. Brabec, and J. Bernholc, Phys. Rev. Lett. **76**, 2511 (1996).
4 H. Dai, Acc. Chem. Res. **35**, 1035 (2002).
5 J. W. G. Wildöer, L. C. Venema, A. G. Rinzler, R. E. Smalley, and C. Dekker, Nature **391**, 59 (1998).
6 C. Dekker, Phys. Today **52**, 22 (1999).
7 P. Kim, L. Shi, A. Majumdar, and P. L. McEuen, Phys. Rev. Lett. **87**, 215502 (2001).
8 C. Yu, L. Shi, Z. Yao, D. Li, and A. Majumdar, Nano Lett. **5**, 1842 (2005).
9 M. Fujii, X. Zhang, H. Xie, H. Ago, K. Takahashi, T. Ikuta, H. Abe, and T. Shimizu, Phys. Rev. Lett. **95**, 065502 (2005).
10 C. W. Chang, D. Okawa, H. Garcia, A. Majumdar, and A. Zettl, Phys. Rev. Lett. **101**, 075903 (2008).
11 J. Yang, S. Waltermire, Y. Chen, A. A. Zinn, T. T. Xu, and D. Li, Appl. Phys. Lett. **96**, 023109 (2010).
12 M. T. Pettes and L. Shi, Adv. Funct. Mater. **19**, 3918 (2009).
13 H. Hayashi, T. Ikuta, T. Nishiyama, and K. Takahashi, J. Appl. Phys. **113**, 014301 (2013).
14 H. Hayashi, K. Takahashi, T. Ikuta, T. Nishiyama, Y. Takata, and X. Zhang, Appl. Phys. Lett. **104**, 113112 (2014).
15 E. Pop, Nano Res. **3**, 147 (2010).
16 C. Meng, C. Liu, and S. Fan, Adv. Mater. **22**, 535 (2010)
17 E. Dujardin, T. W. Ebbesen, H. Hiura, and K. Tanigaki, Science **265**, 1850 (1994).
18 B. M. Kim, S. Sinha, and H. H. Bau, Nano Lett. **4**, 2203 (2004).
19 J. A. Thomas, R. M. Iutzi, and A. J. H. McGaughey, Phys. Rev. B **81**, 045413 (2010).
20 G. Zhang, W. Wang, and X. Li, Adv. Mater. **20**, 3654 (2008).
21 J. Kang, J. W. Roh, W. Shim, J. Ham, J.-S. Noh, and W. Lee, Adv. Mater. **23**, 3414 (2011).
22 M. Hu, X. Zhang, K. P. Giapis, and D. Poulikakos, Phys. Rev. B **84**, 085442 (2011).
23 M. C. Wingert, Z. C. Y. Chen, E. Dechaumphai, J. Moon, J.-H. Kim, J. Xiang, and R. Chen, Nano Lett. **11**, 5507 (2011).
24 X. Zhang, H. Xie, M. Fujii, H. Ago, K. Takahashi, T. Ikuta, H. Abe, and T. Shimizu, T. Appl. Phys. Lett. **86**, 171912 (2005).
25 T. Welton, Chem. Rev. **99**, 2071 (1999).
26 M. G. Freire, P. J. Carvalho, A. M. Fernandes, I. M. Marrucho, A. J. Queimada, and J. A. P. Coutinho, J. Colloid Interface Sci. **314**, 621 (2007).

27 T. W. Ebbesen, J. Phys. Chem. Solids **57**, 951 (1996).
28 S. Chen, G. Wu, M. Sha, and S. Huang, J. Am. Chem. Soc. **129**, 2416 (2007).
29 G. Brown, S. R. Bailey, M. Novotny, R. Carter, E. Flahaut, K. S. Coleman, J. L. Hutchison, M. L. H. Green, and L. Sloan, Appl. Phys. A **76**, 457 (2003).
30 L. Shi, D. Li, C. Yu, W. Jang, D. Kim, Z. Yao, P. Kim, and A. Majumdar, J. Heat Transfer **125**, 881 (2003).
31 K. Takahashi, Y. Ito, T. Ikuta, X. Zhang, and M. Fujii, Physica B: Condensed Matter **404**, 2431 (2009).
32 A. Askounis, Y. Yamada, T. Ikuta, K. Takahashi, Y. Takata, and K. Sefiane, AIP Advances **6**, 115119 (2016)
33 M. Endo, Y. A. Kim, T. Hayashi, Y. Fukai, K. Oshida, M. Terrones, T. Yanagisawa, S. Higaki, and M. S. Dresselhaus, Appl. Phys. Lett. **80**, 1267 (2002).
34 T. L. Bergman, F. P. Incropera, D. P. DeWitt, and A. S. Lavine, Fundamentals of Heat and Mass Transfer. (Wiley, 2011).
35 A. M. Marconnet, M. A. Panzer, and K. E. Goodson, Rev. Mod. Phys. **85**, 1295 (2013).
36 M. E. V. Valkenburg, R. L. Vaughn, M. Williams, and J. S. Wilkes, Thermochim. Acta **425**, 181 (2005).
37 A. P. Fröba, M. H. Rausch, K. Krzeminski, D. Assenbaum, P. Wasserscheid, and A. Leipertz, Int. J. Thermophys. **31**, 2059 (2010).
38 K. Dong, G. Zhau, X. Liu, X. Yao, S. Zhang, and A. Lyubartsev, J. Phys. Chem. C **113**, 10013 (2009).
39 R. Singh, J. Monk, and F. R. Hung, J. Phys. Chem. C **114**, 15478 (2010).
40 N. Mingo and D. A. Broido, Nano Lett. **5**, 1221 (2005).
41 A. L. Moore, and L. Shi, Mater. Today, **17**, 163 (2014).
42 T. Mai, and O. Narayan, Phys. Rev. E, **73**, 061202 (2006).